Physica B 488 (2016) 43–48

Contents lists available at ScienceDirect

Physica B

journal homepage: www.elsevier.com/locate/physb

Synthesis of stoichiometric $Ca_2Fe_2O_5$ nanoparticles by high-energy ball milling and thermal annealing

B.F. Amorim [a], M.A. Morales [a], F. Bohn [a], A.S. Carriço [a], S.N. de Medeiros [a,*], A.L. Dantas [b]

[a] Departamento de Física Teórica e Experimental, Universidade Federal do Rio Grande do Norte, 59078-900 Natal, RN, Brazil
[b] Departamento de Física, Universidade do Estado do Rio Grande do Norte, 59610-210 Mossoró, RN, Brazil

ARTICLE INFO

Article history:
Received 2 November 2015
Received in revised form
22 January 2016
Accepted 26 January 2016
Available online 3 February 2016

Keywords:
Dicalcium ferrite
High-energy ball milling
Mössbauer spectroscopy
X-ray diffraction
Magnetic nanoparticles

ABSTRACT

We report the synthesis of $Ca_2Fe_2O_5$ nanoparticles by high-energy ball milling and thermal annealing from α-Fe_2O_3 and $CaCO_3$. Magnetization measurements, Mössbauer and X-ray spectra reveal that annealing at high temperatures leads to better quality samples. Our results indicate nanoparticles produced by 10 h high-energy ball milling and thermal annealing for 2 h at 1100 °C achieve improved stoichiometry and the full weak ferromagnetic signal of $Ca_2Fe_2O_5$. Samples annealed at lower temperatures show departure from stoichiometry, with a higher occupancy of Fe^{3+} in octahedral sites, and a reduced magnetization. Thermal relaxation for temperatures in the 700–1100 °C range is well represented by a Néel model, assuming a random orientation of the weak ferromagnetic moment of the $Ca_2Fe_2O_5$ nanoparticles.

1. Introduction

Perovskite type oxides are promising systems as candidates for the replacement of catalysis containing noble metals in a number of high-temperature oxidation processes [1]. In particular, catalytic combustion of C_3H_6 and other volatile organic compounds over perovskite-type oxides has been studied for several decades [2].

Dicalcium ferrite, $Ca_2Fe_2O_5$, is usually considered as anion-deficient perovskite with ordered oxygen vacancies, in which the main structural modification consists of alternating octahedral and tetrahedral layers [1]. The structure permits the accommodation of a several metal cations of different valences and has an unusual capacity to support a number of different types of defects [2]. Furthermore, such systems display a wide variety of interesting effects, they are also used to test models for simple antiferromagnets through the investigation of many-sublattice antiferromagnets [3].

Coprecipitation, ceramic methods and the free float zone technique have been employed for the synthesis of powder and single crystals of $Ca_2Fe_2O_5$ [1,4]. However, less attention has been devoted to the high-energy ball-milling (HEBM) technique. HEBM technique has emerged as a non-expensive route to produce non-equilibrium phases in several forms, such as amorphous and nanostructured materials, nanocomposites and extended solid solutions. In this case, metastable phases are usually produced when the raw materials are submitted to fracturing, deformation, and welding, due to the introduction of free energy in the crystal lattice during the milling process [5].

In this paper we report the synthesis of dicalcium ferrite prepared by high energy ball-milling from stoichiometric amounts of the $CaCO_3$ and Fe_2O_3 precursors, in an air atmosphere, followed by thermal annealing. The structural and magnetic characterization of the resulting powders are investigated and analyzed through X-ray diffraction, magnetization measurements, Mössbauer spectroscopy, and a theoretical model to describe the magnetic behavior.

2. Experiment

For this study, dicalcium ferrite samples, with nominal composition $Ca_2Fe_2O_5$, were prepared in a planetary ball-mill (Fritsch Pulverisette 7 – Premium line), with vial and balls of hardened steel, in air atmosphere, followed by thermal annealing. Analytical grade α-Fe_2O_3 and $CaCO_3$ (calcite) powders, both purchased from Sigma-Aldrich, were used as precursors, with relative weight amount of 44% and 56%, respectively. The ball-to-powder mass ratio (BPMR) was 30:1, and the angular velocity of the supporting disc and vial was 300 rpm, both were kept constant throughout the experiments. The balls and powder are placed in the vial in the presence of air and are effectively milled during 10 and 80 h, in which 1 h milling periods are alternated with 10 min rest periods to reduce the heating. Then, the

* Corresponding author.
E-mail address: sndemedeiros@gmail.com (S.N. de Medeiros).

http://dx.doi.org/10.1016/j.physb.2016.01.029
0921-4526/

10 h milled powders were annealed in air atmosphere at 700 °C, 900 °C and 1100 °C, during 2 h.

Phase characterization of the produced powders was carried out via X-ray diffraction (XRD) using a Rigaku MiniFlex II diffractometer, with CuKα radiation of $\lambda = 1.54$ Å. The XRD patterns were refined by the Rietveld method using the program MAUD, providing the lattice parameters and phase fractions. The crystallite size was determined by using the Scherrer formula [6].

Magnetization measurements were performed using a homemade vibrating sample magnetometer (VSM), at room temperature, with maximum field of 1.5 T.

Finally, Mössbauer spectra (MS) were recorded in transmission mode at room temperature using a conventional spectrometer in a constant acceleration mode, with gamma rays provided by ^{57}Co(Rh) source. The MS were analyzed using a non-linear least-square routine, with Lorentzian line shape. Isomer shift values are related to α-Fe at 300 K.

3. Results and discussion

3.1. XRD analysis

Fig. 1 shows the X-ray diffraction results for the unmilled sample, samples milled during 10 h and 80 h, as well as for the samples milled during 10 h and annealed at different temperatures.

For the unannealed samples (Fig. 1(a)–(c)), the patterns indicate only phases related to α-Fe_2O_3 and hexagonal calcite. In each diffractogram, the reflection peaks for α-Fe_2O_3 (71194-ICSD) and calcite $CaCO_3$(40543-ICSD) are greatly broadened as a consequence of grain size refinement and of disordered/defective structure. Table 1 presents the crystalline parameters and fractions of the phases obtained from the refinement procedure. For both phases, the grain size decreases with the milling time, while the lattice parameters are slightly different than that found in literature. (The reference ICSD lattice parameters values are presented in the first column of Table 1.) The fractions of the phases change after milling, and this fact may be related to the lost of a fraction of the $CaCO_3$ material. In fact, we have noticed the formation of deposits on the vial and spheres surface, which may be related to the $CaCO_3$ phase. Notice that the high-energy ball milling procedure does not produce detectable amount of the $Ca_2Fe_2O_5$ phase.

Considering the annealed samples (Fig. 1(d)–(f)), the results now disclose peaks unequivocally identified as being for the $Ca_2Fe_2O_5$ (88990-ICSD) phase. In particular, in these samples, no second phase is verified. The crystalline parameters for the $Ca_2Fe_2O_5$ samples are shown in Table 2. The crystallite size and lattice parameter slightly increases with the annealing temperature, a trend in agreement with the crystallite growth and reduction of the disordered/defective structure.

Since a high-energy milling system was used to produce the samples, one could figure that some Fe contamination from the steel vial or balls may be possible. Furthermore, reports on reduction of pure hematite to Fe^{2+} containing phase via ball milling can be found in literature. For instance, $Fe_{1-x}O_x$ phase was obtained from hematite after milling for periods from 3 h to 10 h, with BPMR ranging from 20 up to 35 and with velocity of 400 rpm [7].

Fig. 2 shows the X-ray pattern for the 80 h milled sample, together with the expected angular positions for the highest intensity peaks in polycrystalline Fe and FeO phases, as well as with simulated patterns for hematite and the $CaCO_3$ polymorphs (calcite (40543-ICSD), aragonite (15194-ICSD) and vaterite (18127-ICSD)). The experimental diffractograms do not suggest any feature that may resemble α-Fe, as well as the second less intense (200)-FeO phase peak is also absent, removing the hypothesis of

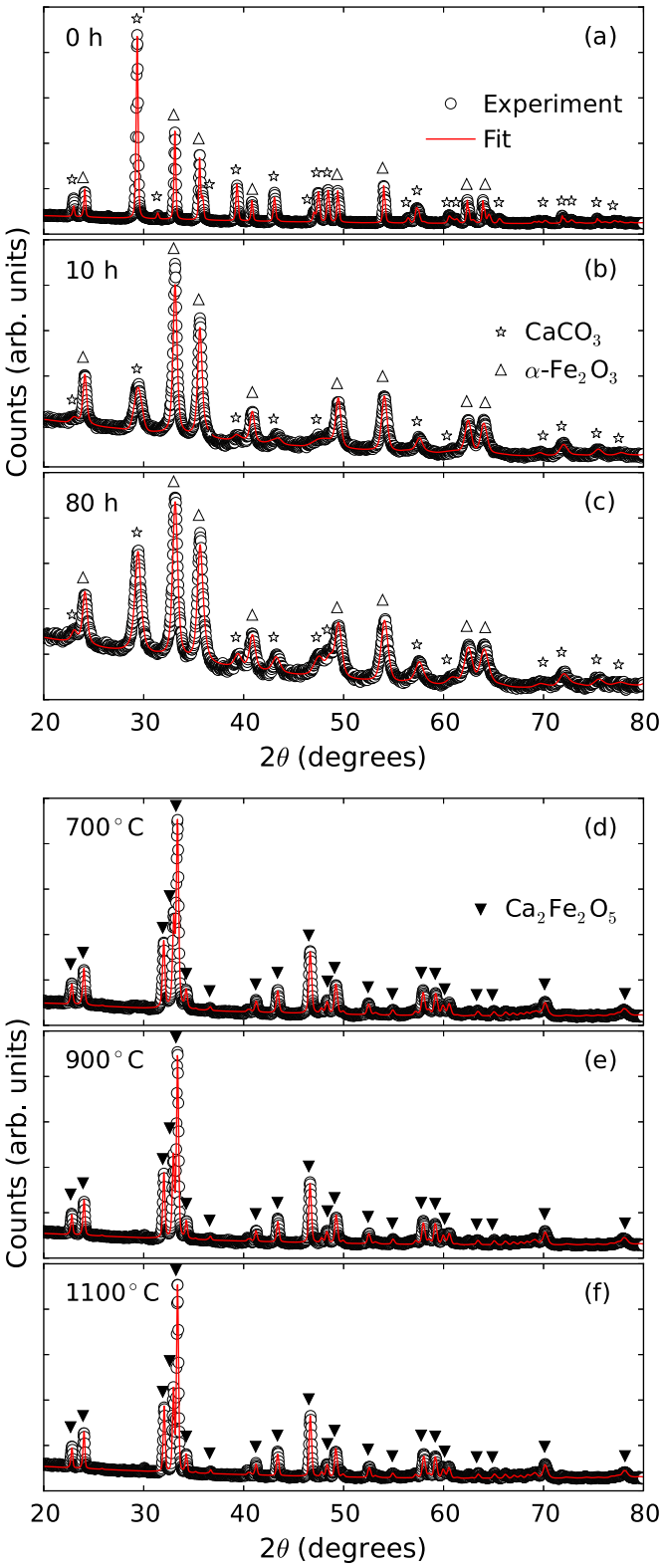

Fig. 1. XRD results for the (a) unmilled samples, samples milled for (b) 10 h and (c) 80 h. Similar plot for samples milled during 10 h and annealed at temperatures of (d) 700 °C, (e) 900 °C, and (f) 1100 °C. The red lines are the fits obtained using the Rietveld method, while the symbols correspond to the peaks indexed for each phase. (For interpretation of the references to color in this figure caption, the reader is referred to the web version of this paper.)

contamination or Fe^{3+} reduction. This result may be associated to the fact that the $CaCO_3$ tend to form deposits on metal surfaces, forming a shell around the balls and the vial, therefore, preventing

Table 1
Crystalline parameters obtained for the unmilled and milled samples.

Phase	Milling time (h)	Crystallite size (nm)	Lattice parameter (Å)		Phase fraction (%)
			a	*c*	
$CaCO_3$	0	141.8	4.999	17.071	–
a=4.988 Å	10	92.6	4.988	17.002	46.1
c=17.061 Å	80	18.1	4.984	17.027	29.2
α-Fe_2O_3	0	140.6	5.039	13.761	–
a=5.035 Å	10	33.6	5.036	13.754	53.9
c=13.750 Å	80	26.4	5.034	13.750	70.8

Table 2
Crystalline parameters for the annealed samples.

Phase	Annealing temperature (°C)	Crystallite size (nm)	Lattice parameter (Å)		
			a	*b*	*c*
$Ca_2Fe_2O_5$	700	30.4	5.563	14.738	5.403
	900	37.1	5.564	14.736	5.409
	1100	39.4	5.570	14.777	5.419

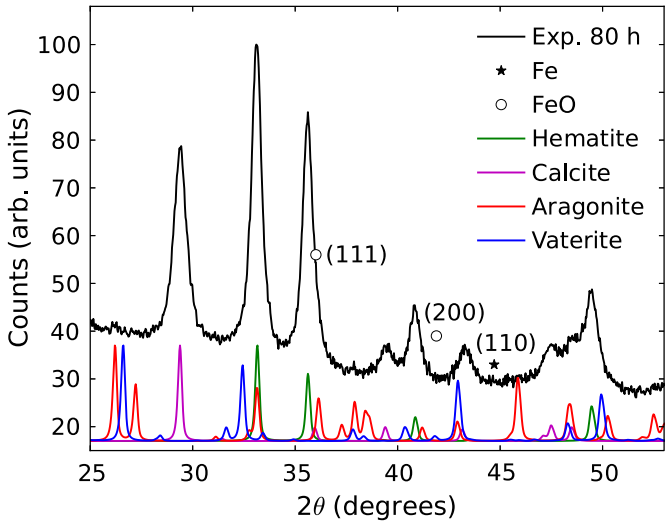

Fig. 2. XRD results for sample milled during 80 h. Circles and star are indications of the expected angular position of the main XRD peaks for the FeO and Fe phases, respectively. The solid lines are simulated patterns for the hematite and $CaCO_3$ polymorphs (calcite, aragonite, and vaterite).

the release of steel debris on the milled powder. However, so far, the understanding on the formation of $CaCO_3$ deposits on metal surfaces is far from complete and more studies are required [8].

Moreover, the milled samples do not present any phase distinct of hematite and calcite. Calcite and aragonite are the most frequent $CaCO_3$ polymorphs. The production of aragonite from calcite by high energy ball milling has been reported for 200 rpm and at the very high BPMR of 60 [9]. In fact, the BPMR is one of the important variables for the milling operation. It plays significant effects on time required to obtain a fine particle from powder and to introduce microstrains. The higher the BPMR the shorter the time required. At high BPMR, the collision of ball in the grinding medium increases per unit time, evolving more energy that lead to the phase transformation to aragonite. If present, polycrystalline aragonite and vaterite should contribute with their most intense peaks, localized between 25° and 28°. However, these peaks are also absent in the 80 h milled sample. The 10 h and 80 h samples have similar difractograms. Thus, all features discussed for the

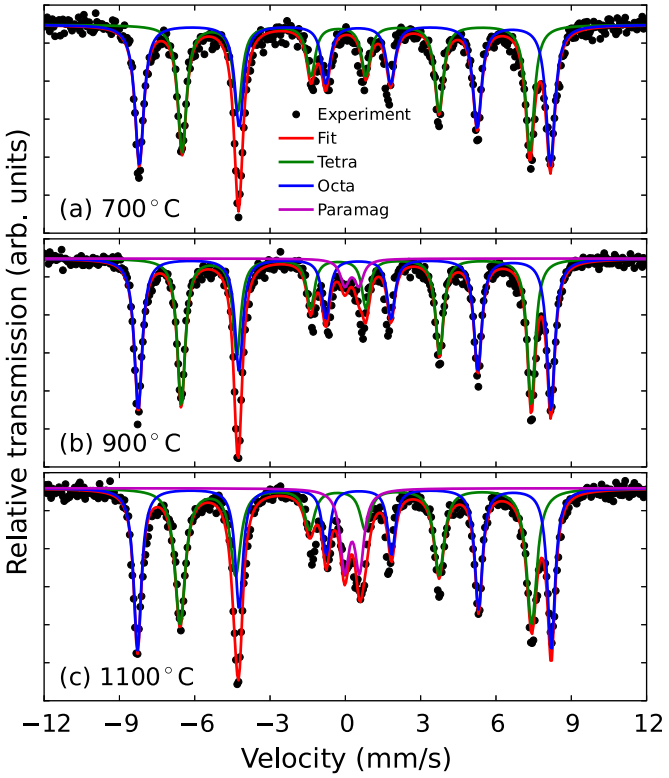

Fig. 3. MS for samples milled by 10 h and annealed at temperatures of (a) 700 °C, (b) 900 °C, and (c) 1100 °C.

80 h milled sample are also valid for the 10 h milled one.

3.2. Mössbauer characterization

Fig. 3 shows the room temperature Mössbauer spectra for the samples annealed at temperatures of 700 °C, 900 °C and 1100 °C, after milling for 10 h.

$Ca_2Fe_2O_5$ is antiferromagnetic, with Néel temperature of 725 K [10]. Thus the MS of blocked particles should exhibit a magnetic splitted spectrum. The MS revealed that the $Ca_2Fe_2O_5$ phase was the main product in the annealed samples, with ferric ions occupying tetrahedral and octahedral symmetry sites. These subspectra exhibit a Zeeman interaction effect, due to the effective hyperfine magnetic field sensed by the ^{57}Fe nucleus, and an electric quadrupolar interaction due to the electric field gradient acting on the nucleus quadrupole moment. The spectra were fitted to two sextets, whose relative absorption areas (RAA) showed equal values for the 1100 °C sample. If we assume that the octahedral and tetrahedral recoilless fractions are similar at room temperature, one can conclude that both sites have similar concentration of Fe^{3+}, as expected for stoichiometric $Ca_2Fe_2O_5$ phase [10]. The rate RAA(octa)/RAA(tetra) for 700 °C, 900 °C and 1100 °C samples were of 1.13, 1.11 and 1.0, indicating that the stoichiometry of $Ca_2Fe_2O_5$ nanoparticles is improved as higher the annealing temperature.

Mössbauer parameters are reported in Table 3. In particular, they resemble to those reported by Randhawa and Sweety [11] for the $Ca_2Fe_2O_5$ phase. There is a paramagnetic doublet in the samples annealed at 900 °C and 1100 °C. The absorption area for this component increased with the annealing temperature, having a maximum value of 12%. Inspecting carefully the X-ray difractogram we could not find a second phase that can be related to the paramagnetic component. This subspectra may be related to very poor crystallinity residues accumulated at the grain boundaries.

Table 3
Magnetization, obtained from analysis of the magnetization curves, and Mössbauer parameters for the produced $Ca_2Fe_2O_5$ nanoparticles.

Annealing temperature (°C)	Component	RAA (%)	IS (mm/s)	$\Delta\epsilon$ (mm/s)	Bhf (T)	M (17 kOe) (emu/g)
700	Tetra	47	0.18	0.70	43	0.133
	Octa	53	0.35	−0.53	51	
	Para	–	–	–	–	
900	Tetra	45	0.19	0.72	43	0.195
	Octa	50	0.35	−0.55	51	
	Para	5	0.37	0.56	–	
1100	Tetra	44	0.16	0.74	43	0.219
	Octa	44	0.36	−0.58	51	
	Para	12	0.38	0.59	–	

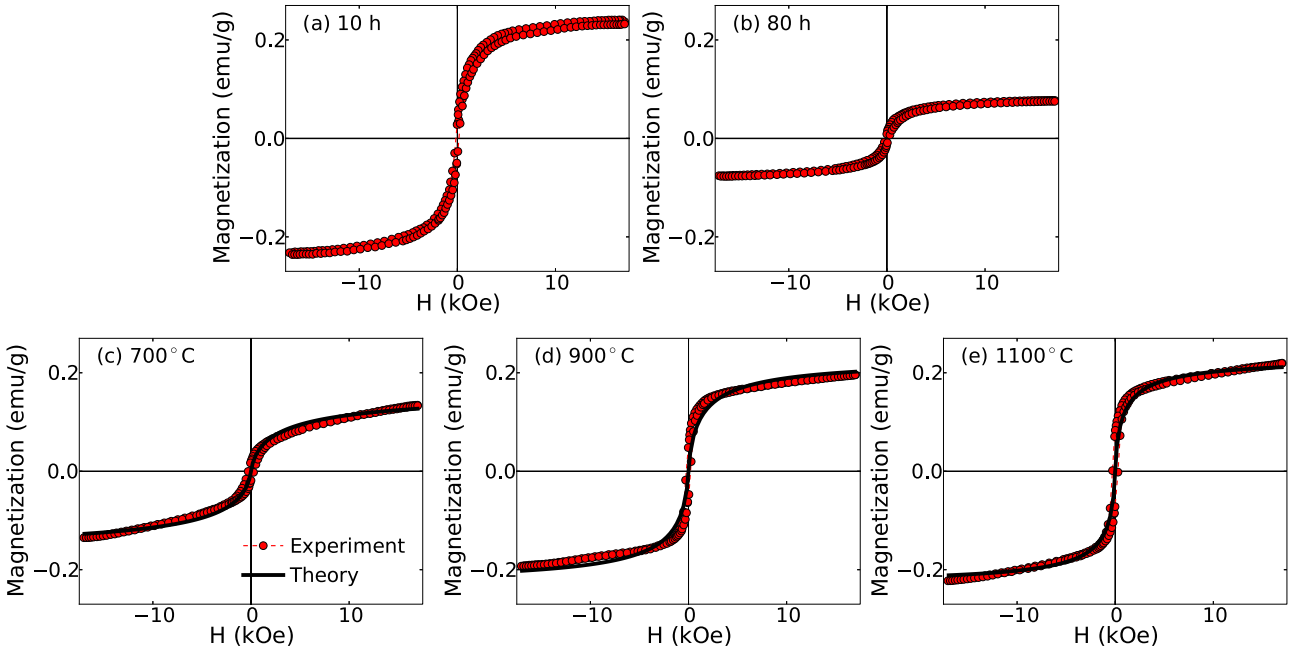

Fig. 4. Magnetization curves measured at 300 K for the samples milled during for (a) 10 h and (b) 80 h, and similar plot for the $Ca_2Fe_2O_4$ nanoparticles produced by 10 h high energy ball milling and annealing of (c) 700 °C, (d) 900 °C and (e) 1100 °C. In (c)–(e) the red circles correspond to the experiment, while the black solid lines are the theoretical results. (For interpretation of the references to color in this figure caption, the reader is referred to the web version of this paper.)

3.3. Magnetization

Fig. 4 shows the magnetization curves at room temperature for the milled and annealed samples. For the samples milled for 10 h and 80 h (Fig. 4(a) and (b)), the samples are ferromagnetic due to the weak ferromagnetic behavior of the hematite [12]. With the increase of the milling time and the decrease of the particle size, the saturation magnetization is reduced drastically from 0.24 to 0.08 emu/g, a fact related to the large total surface and canting of the magnetic moments [13].

Regarding the annealed samples (Fig. 4(c)–(e)), they have larger values of initial susceptibility and of the magnetization for large external field strengths, as also shown in Table 3.

Previous works show that the magnetization of $Ca_2Fe_2O_5$, measured at 20 K under a magnetic field strength of 5 kOe, is around 0.27 emu/g [3]. Our results, shown in Fig. 4, reveals that the magnetization of the sample annealed at 700 °C, measured at an external field strength of $H=17$ kOe, is about 49% of the value reported in [3]. Furthermore, the magnetization does not saturate for large values of the external field strength. These results are signatures of thermal relaxation of small size nanoparticle systems [14].

The easy axis direction of $Ca_2Fe_2O_5$ is parallel to the a-axis [3]. We assume our samples consist of weak ferromagnetism single domain $Ca_2Fe_2O_5$ nanoparticles, with the magnetic moment along the easy axis direction. In the vibrating sample magnetometer sample holder, the nanoparticles have random orientation of the a-axis with respect to the direction of the external field. Therefore the thermal relaxation at room temperature may be estimated using a Langevin function [15].

For a given value of the external field, the magnetization is given by:

$$M(H) = M_S \int \mathcal{L}\{\mu(D)H/k_BT\} f(D)\, dD, \quad (1)$$

where $\mathcal{L}$ is the Langevin function, M_S is the saturation magnetization, $\mu(D) = \pi M_S D^3/6$ is the saturation magnetic moment of a nanoparticle of diameter D, H is the external field strength, and f is a log-normal distribution function.

As shown in Fig. 4(c)–(e), the susceptibility of the low temperature sample is 0.064 emu/(g kOe) and that of the 1100 °C sample, 0.166 emu/(g kOe). The initial susceptibility of the 1100 °C sample is a factor of 2.6 larger than that of the 700 °C sample. This may be interpreted as indicative that the 1100 °C sample is made of larger nanoparticles, in comparison to the 700 °C sample. As we shall discuss below, our samples consist of nanoparticles with a polydisperse, moderately wide size distribution. However, before the detailed discussion of the impact of the annealing temperature on the size distribution functions, it is instructive to consider a rather simple model, consisting of a monodisperse nanoparticle system. This allows us making a preliminary estimative of the

impact of the annealing temperature on the nanoparticles size.

A monodisperse system has a thermal average magnetic moment given by:

$$\mu = \mu_0 \mathcal{L}\{\mu_0 H/k_B T\}, \quad (2)$$

where μ_0 is the saturation moment. For a spherical nanoparticle of diameter D, $\mu_0 = \pi D^3 m_0/6$, $m_0 = \rho M_S^0$ is the magnetic moment per cm^3 and $\rho = 4.01$ g/cm^3 is the $Ca_2Fe_2O_5$ density.

The initial susceptibility is given by

$$\chi = \frac{\mu_0^2}{3K_B T}. \quad (3)$$

Assuming that m_0 is the same, we may anticipate that the 1100 °C sample nanoparticles diameter are 20% larger than those of the 700 °C sample. This rather simple estimative is close to what may be found from the X-ray data. The X-ray line widths indicate a 1.3 ratio of the average crystallite sizes.

For the investigation of particle size distribution parameters in ferrofluids, quantitative studies using several models for ideal and interacting particles have been performed [16,17] to select the best distribution functions for magneto-granulometric analysis as well as for accurately reproducing key magnetic parameters and macroscopic quantities.

Previous reports indicate that the dipolar interaction between superparamagnetic sodium oleate coated magnetite nanoparticles may have a large impact on the initial susceptibility [18]. It has been shown that the dipolar interaction between the magnetite nanoparticles plays a key role in the magnetic response to external field in the mT range, and leads to the large value of the initial susceptibility. The enhancement of the initial susceptibility has been attributed to the dipolar field produced by the superparamagnetic nanoparticles. It has been shown that for small values of the external field strength, the thermal average value of each nanoparticle's magnetic moment is small, but enough to produce a dipolar field of the order of the external field strength.

Dipolar effects have also been reported for magnetite nanoparticle systems produced by high-energy ball milling [19]. In this case the samples consist of bare magnetite nanoparticles, with no coating, and the dipolar interaction between the nanoparticles is stronger. It has been shown that the dipolar interaction between the magnetite nanoparticles leads to coercivity at room temperature, for magnetite nanoparticles systems with dimensions in the superparamagnetic regime.

In both cases [18,19] the impact of the nanoparticles dipolar interaction on the magnetization curves at room temperature originates in the fact that in the VSM sample holder the nanoparticles are in close contact. Bulk magnetite has a room temperature magnetization of the order of 92 emu/g [15], which is much larger than the magnetization of $Ca_2Fe_2O_5$ at 20 K, which is around 0.27 emu/g [3]. Therefore the $Ca_2Fe_2O_5$ nanoparticles dipolar interaction has been neglected in our present study.

We have assumed that departures from stoichiometry, and surface effects, may lead to reduction of the nanoparticles saturation magnetic moment. For each sample we have used a log-normal distribution function:

$$f(D) = \frac{1}{\sqrt{2\pi}\sigma D} \exp\left[\frac{-\ln(D/D_0)^2}{2\sigma^2}\right] \quad (4)$$

where the standard deviation σ, the median diameter D_0, and the magnetic moment per unit volume m_0 were adjusted to reproduce the magnetization curves.

The values of the standard deviation σ, the median diameter D_0, and the magnetic moment per unit volume m_0 were chosen to fit the initial susceptibility and the asymptotic behavior of the magnetization curves at large values of the external field strength. Furthermore, in choosing the size distribution function parameters (σ and D_0), we have used the data from the X-ray spectra, regarding the crystallite size. For the magnetic moment per unit volume m_0, we have used the Mössbauer spectra data. For instance, a nearly perfect stoichiometry, with equal population of octahedral and tetrahedral sites by the Fe^{3+} ions, is indicative that m_0 should be close to the bulk value.

For the 700 °C sample, we have used $\sigma = 0.55$ and a $D_0 = 40.0$ nm median diameter, and $M_S = 0.60 M_S^0$. The nanoparticles have a 40% reduction of the magnetization. Most of the nanoparticles have a 30 nm diameter. Furthermore, 80% of the nanoparticles have diameters in the 12–65 nm range. This is consistent with the data from the X-ray and the Mössbauer spectra, which indicates crystallite size around 30.4 nm and a damaged stoichiometry, with unequal population of octahedral and tetrahedral sites by the Fe^{3+} ions.

The magnetization of the high temperature samples, with larger nanoparticles, a small reduction of the magnetization is verified, $M_S = 0.84 M_S^0$. For these samples, we have used $\sigma = 0.50$, and median diameters of $D_0 = 47.0$ nm and $D_0 = 56.0$ nm. For the 900 °C sample, 80% of the nanoparticles have diameters in the 12–73 nm range, and most of the nanoparticles have a 37 nm diameter. For the 1100 °C sample, most of the nanoparticles have a 43 nm diameter and 80% of the nanoparticles have diameters in the 12–87 nm range. This is consistent with the data from the X-ray spectra, which indicates crystallite size around 37.1 nm and 39.4 nm. The small reduction of magnetization is as expected for a nearly perfect stoichiometry, with equal population of octahedral and tetrahedral sites by the Fe^{3+} ions, as seen in the Mössbauer spectra.

4. Conclusion

We have synthesized $Ca_2Fe_2O_5$ nanoparticles by high-energy ball milling and thermal annealing from α-Fe_2O_3 and $CaCO_3$. Our results indicate that high temperature annealing leads to better quality nanoparticles, with relevant stoichiometry improvement, as seen from the MS in the Fe^{+3} population of octahedral and tetrahedral sites, and a clear signature of the weak ferromagnetism of $Ca_2Fe_2O_5$, as seen in the magnetization curves. Stoichiometric $Ca_2Fe_2O_5$ nanoparticles were obtained after 10 h milling and thermal annealing for 2 h at 1100 °C.

Acknowledgments

The authors acknowledge financial support from CAPES, FAPERN and CNPq.

References

[1] L.A. Isupova, S.V. Tsybulya, G.N. Kryukova, A.A. Budneva, E.A. Paukshtis, G. S. Litvak, V.P. Ivanov, V.N. Kolomiichuk, Y.T. Pavlyukhin, V.A. Sadykov, Mechanochemical synthesis and catalytic properties of the calcium ferrite $Ca_2Fe_2O_5$, Kinet. Catal. 43 (2002) 122–128.

[2] D. Hirabayashi, T. Yoshikawa, K. Mochizuki, K. Suzuki, Y. Sakai, Formation of brownmillerite type calcium ferrite ($Ca_2Fe_2O_5$) and catalytic properties in propylene combustion, Catal. Lett. 110 (2006) 269–274.

[3] P. Marchukov, R. Geick, C. Brotzeller, W. Treutmann, E.G. Rudashevsky, A. M. Balbashov, Static magnetic properties of the many-sublattice antiferromagnet $Ca_2Fe_2O_5$, Phys. Rev. B 48 (1993) 13538–13546.

[4] M. Ceretti, A. Piovano, A. Cousson, T. Berthier, M. Meven, G. Agostini, J. Schefer, O. Hernandez, C. Lamberti, W. Paulus, Static magnetic properties of the many-sublattice antiferromagnet $Ca_2Fe_2O_5$, Cryst. Eng. Commun. 14 (2012) 5771–5776.

[5] C. Suryanarayana, Mechanical alloying and milling, Prog. Mater. Sci. 46 (2001) 1–184.

[6] B.D. Cullity, Elements of X-ray Diffraction, 3rd ed., Pretence Hall, Reading, 2001.
[7] M. Zdujić, Č. Jovalekić, Lj. Karanović, M. Mitrić, The ball milling induced transformation of α-Fe_2O_3 powder in air and oxygen atmosphere, Mater. Sci. Eng. A 262 (1999) 204–213.
[8] H. Wang, V. Alfredsson, J. Tropsch, R. Ettl, T. Nylander, Formation of $CaCO_3$ deposits on hard surfaces—effect of bulk solution conditions and surface properties, Appl. Mater. Interfaces 5 (2013) 4035–4045.
[9] H. Pesenti, M. Leoni, P. Scardi, XRD line profile analysis of calcite powders produced by high energy milling, Z. Kristallogr. Suppl. 27 (2008) 143–150.
[10] M. Eibschütz, U. Ganiel, S. Shtrikman, Mössbauer and magnetic studies of dicalcium ferrite ($Ca_2Fe_2O_5$), J. Mater. Sci 4 (1969) 574–580.
[11] B.S. Randhawa, K. Sweety, Calcium ferrite formation from the thermolysis of calcium tris (maleato) ferrate(III), Bull. Mater. Sci. 23 (2000) 305–307.
[12] R.M. Cornell, U. Schwertmann, The Iron Oxides, VCH, Weinheim, Cambridge, 2003.
[13] S. Mørup, E. Brok, C. Frandsen, Spin structures in magnetic nanoparticles, J. Nanomater. 2013 (2013) 720629.
[14] B. Veriansyah, J.D. Kim, B.K. Min, J. Kim, Continuous synthesis of magnetite nanoparticles in supercritical methanol, Mater. Lett. 64 (2010) 2197–2200.
[15] J.M.D. Coey, Magnetism and Magnetic Materials, Cambridge University Press, New York, 2010.
[16] M. Rasa, Magnetic properties and magneto-birefringence of magnetic, Fluids Eur. Phys. J. E 2 (2000) 265–275.
[17] R.W. Chantrell, J. Popplewell, S.W. Charles, Measurements of particle size distribution parameters in ferrofluids, IEEE Trans. Magn. 14 (1978) 975.
[18] R.P. Araújo-Neto, E.L. Silva-Freitas, J.F. Carvalho, T.R.F. Pontes, K.L. Silva, I.H. M. Damasceno, E.S.T. Egito, A.L. Dantas, M.A. Morales, A.S. Carriço, Monodisperse sodium oleate coated magnetite high susceptibility nanoparticles for hyperthermia applications, J. Magn. Magn. Mater. 364 (2014) 72.
[19] R.J.F. de Carvalho, S.N. de Medeiros, M.A. Morales, A.L. Dantas, A.S. Carriço, Synthesis of magnetite nanoparticles by high energy ball milling, Appl. Surf. Sci. 275 (2013) 84.